Doppler Tomography:
It's easy, it's fun, and everybody should try it.

Keith Horne, STScI

To appear in : *Fundamental Properties of Cataclysmic Variable Stars: 12th North American Workshop on Cataclysmic Variables and Low Mass X-ray Binaries. San Diego 3-5 Jan 1991.*
ed. A. W. Shafter (San Diego State University Publication).

Abstract

Doppler tomography is a method that can be used to reorganize observational data to form useful visualizations of line-forming regions in a binary star system. The required observational data are velocity profiles at different binary phases. The doppler-broadened line profile offers a projection of the velocity distribution onto the observer's line of sight, while rotation of the binary presents the observer with a continuously varying sequence of velocity projections. This combination of doppler shifting and binary rotation provides sufficient information for the assembly of 2-dimensional doppler maps. The situation is analogous to the CAT scan used in medical imaging.

Powerful maximum entropy methods have been developed for reconstructing doppler maps using emission lines from accretion disks in cataclysmic variable stars (Marsh and Horne 1988), and absorption lines from the photospheres of spotted stars (Vogt, Penrod and Hatzes 1987). We focus here on a simple linear tomography algorithm, the fourier-filtered back-projection (FFBP), which is faster and easier to program than the maximum entropy techniques. Availability of this fast simple algorithm should help to promote more widespread applications of doppler mapping.

Doppler maps of cataclysmic variables show broad rings of emission from gas orbiting at various radii in the accretion disk, sharp peaks from the active chromosphere of the companion star, and streaks tracing the gas stream flowing from the companion star to the disk (Marsh and Horne 1990, Marsh *et al.* 1990). The quiescent accretion disk's $R^{-3/2}$ Balmer-line emissivity profile, inferred from the doppler maps, suggests a connection with the chromospheres of rotating stars, namely that the emission lines represent dynamo-driven magnetic "activity" that scales linearly with the rotation frequency (Horne and Saar 1991).

Basic Concepts

The observational data used in doppler tomography are sets of velocity-resolved line profiles covering a variety of phases around the binary orbit. For identifying subtle patterns in the data, it helps to assemble the spectra into a 2-dimensional trailed spectrogram, $D(v, \phi)$, which may be displayed as a greyscale or false-color image giving the observed flux density as a function of wavelength (or velocity v) and binary phase ϕ. A good collection of trailed spectrograms for cataclysmic variable stars is provided by Honeycutt, Kaitchuck and Schlegel (1987). These typically exhibit double-peaked emission lines from the accretion disk, narrow "S-wave" components (following sinusoidal velocity curves) from the companion star and gas stream, and single-peaked (sometimes blue-shifted) components possibly from winds.

A gas flow that is stationary in the rotating frame of a binary system may be visualized in both position and doppler coordinates. Every parcel of gas has both a position, (X, Y, Z), and a velocity, (V_X, V_Y, V_Z). We refer here to a cartesian coordinate frame rotating with the binary system, and project the velocity vectors (which rotate in the inertial frame) onto the co-rotating coordinate axes. In many interesting cases, for example gas streams and accretion disks resulting from Roche lobe overflow, the small V_Z component allows us to approximate the motion by a 2-dimensional flow confined to the orbital plane.

A doppler map gives the distribution of the emission-line gas in doppler coordinates (V_X, V_Y). The main advantage of making the map in doppler rather than position coordinates is the close relationship between the doppler coordinates and the observed velocity profiles, which makes it possible to construct the doppler map without knowing the precise nature of the velocity field. A disadvantage is that two distinct parcels of gas can have precisely the same doppler coordinates, and this must be kept in mind when interpreting a doppler map.

We will consider two useful ways of thinking about the relationship between the doppler map and the trailed spectrogram data. First, if you project the doppler map along various directions, by integrating between pairs of parallel lines crossing the map, you obtain a set of velocity profiles for each of the corresponding binary phases. These predicted velocity profiles must fit the observed line profiles.

For the second viewpoint, consider each pixel on the doppler map, labelled with its doppler coordinates (V_X, V_Y), as a particular S-wave component that follows a sinusoidal velocity curve $V(V_X, V_Y, \phi) = V_Y \sin(2\pi\phi) - V_X \cos(2\pi\phi)$. A trailed spectrogram is produced by summing up the S-wave components from all the pixels of the doppler map. The map gives the strength of these S-wave components required to fit the observed data.

The Back-Projection Algorithm

How can we construct doppler maps from observational data ? Consider first the simple back-projection (BP) algorithm. Remember that each pixel on the doppler map, specified by its doppler coordinates (V_X, V_Y), is identified with a particular sinusoidal velocity curve $V(V_X, V_Y, \phi)$. To obtain the back-projection $BP(V_X, V_Y)$, simply evaluate (interpolate in v) the flux density from each observed spectrum at the velocity given by the velocity curve, and then average over all the spectra. Thus

$$BP(V_X, V_Y) = \frac{\int D(V(V_X, V_Y, \phi), \phi) w(\phi) d\phi}{\int w(\phi) d\phi}.$$

where $D(v, \phi)$ is the data at velocity v and phase ϕ, and $w(\phi)$ are phase-dependent weights.

One is tempted here to use inverse-variance weights, proportional to the inverse of the variance of the interpolated data, which minimize the statistical uncertainty of the doppler map. However, it is probably better to use $w(\phi)$ to equalize the weighting around the binary orbit, for otherwise "radial spoke" artefacts tend to appear more strongly in the map, as discussed below.

To understand how a back-projection works, consider a dataset consisting of a single strong S-wave emission component. Most pixels on the doppler map correspond to sinusoidal velocity curves that are not exactly aligned with the S-wave in the data. For these pixels, we obtain a relatively small mean flux because the the observed flux along the velocity curve is zero except for two small contributions from the phase intervals during which the velocity curve crosses over the S-wave in the data. However, one place on the doppler map corresponds to the velocity curve that exactly follows the S-wave component in the data. In this case, of course, the mean flux is large because the flux remains high all along the velocity curve. The BP map will therefore have a peak at the velocity coordinates corresponding to the S-wave in the data. Pixels close to the peak will have velocity curves that cross slowly

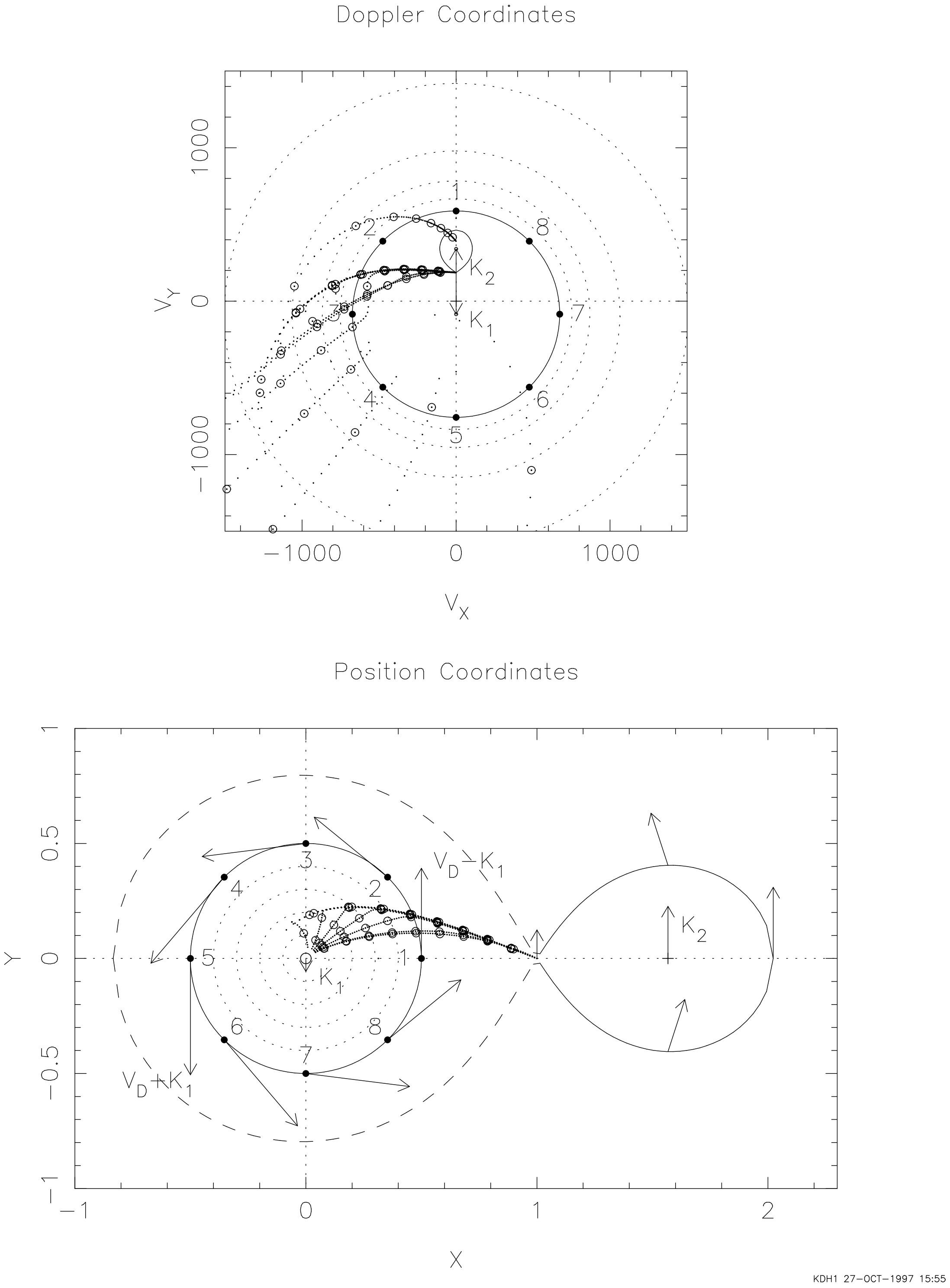

Figure 1: Schematic view of a cataclysmic variable star, including the Roche lobe filling companion star, the mass transfer stream, and the accretion disk around the white dwarf, shown both in spatial coordinates (X,Y), and in the corresponding Doppler coordinates (V_X, V_Y).

over the S-wave in the data, and will therefore receive a higher mean flux than pixels located farther from the peak, whose velocity curves cross rapidly over the S-wave. From further analysis along these lines one can see that the peak in the map will have a gaussian core defined by the spectral resolution of the data, and broad wings with a $1/V$ profile. This is the point-spread function of the back-projection method.

There is a second completely equivalent way of thinking about the back-projection. Start with a blank map. Then, for each observed spectrum, "paint down" the velocity profile from that spectrum as a probability strip across the map at an angle corresponding to the binary phase of that spectrum. For our dataset with a single S-wave component, each spectrum paints down a narrow stripe that is offset from the center of the map by the velocity appropriate to the phase of that spectrum. As the spectra from different phases are applied, the series of probability stripes all cross at a single point, building up a peak at the doppler coordinates of the S-wave in the data.

This "painting down" viewpoint helps in understanding the point-spread function and various artefacts that can arise in doppler maps. For example, it is now obvious that a high pixel in a single spectrum will produce a stripe across the map at an angle corresponding to the binary phase of that spectrum, and offset from the center of the map by the velocity of the high pixel. If the binary phase coverage is non-uniform, for example if too few binary phases are covered in the set of observed spectra, then each peak in the map will be surrounded by a series of radial spokes in the directions of the observed spectra. In general, the point-spread function of the BP map, imposed by the spectral resolution and phase coverage of the data, can be obtained by painting down the weighted resolution elements of all the spectra.

The back-projection algorithm is simple to understand, straightforward to program, and produces maps which are quite acceptable for investigating the kinematics of various S-wave components in the data. However, back-projection has a very serious limitation: it does not give a faithful reconstruction of the data. Projections of a back-projected doppler map give velocity profiles that do not agree with the observed data.

The back-projection algorithm gives the true doppler map convolved with a point-spread function that is best understood by thinking about the back-projection as a painting down of probability stripes from each of the observed spectra. The point-spread function (in the limit of a large number of observed phases) has a gaussian core defined by the velocity resolution of the spectral data, and broad wings with a $1/V$ profile.

The Fourier-Filtered Back-Projection

The fourier-filtered back-projection (FFBP) is a simple extension of the back-projection algorithm that attempts to sharpen up the point-spread function. Simply apply a fourier filter to each of the observed spectra, and then use the back-projection to obtain the doppler map. Applying the fourier filter involves computing the fourier transform of the spectrum ($S(v) \rightarrow \tilde{S}(\omega)$), multiplying the resulting fourier amplitudes $\tilde{S}(\omega)$ by the fourier filter $G(\omega)$, and then inverse fourier transforming ($S'(v) \leftarrow \tilde{S}(\omega)G(\omega)$) to recover the fourier-filtered spectrum $S'(v)$.

The fourier filter needed to correct for back-projection's $1/V$ point-spread function turns out to be a high-pass ramp filter, $G(\omega) = (\omega/\omega_N)$, where ω_N is the nyquist frequency. Each fourier component of the observed spectrum must be amplified in proportion to its fourier frequency ω. Note that, since $G(0) = 0$, the mean value of the spectrum is completely suppressed by the high-pass ramp filter. Thus, in our example of a single S-wave in the data, the mean flux along a velocity curve will be 0 if the velocity curve crosses over the S-wave. It can be shown that this filter yields an exact reconstruction when the data are free of noise, have infinite spectral resolution, and complete phase coverage.

A potential problem with the fourier filter is the amplification of high-frequency noise. This may not be too serious in practice if the signal-to-noise ratio of the data are reasonably high. However, observed spectra generally have a white noise component, and the signal-to-noise ratio can be poor at the highest fourier frequencies. A practical cure is to curtail the high-frequency ramp filter by including a gaussian cutoff. For example, $G(\omega) = (\omega/\omega_N) exp(-(\omega/\omega_c)^2/2)$ will suppress noise above a cutoff frequency ω_c, while preserving the linear ramp for $\omega << \omega_c$. The doppler image obtained with the high-frequency cutoff will have reduced noise, but will also be in effect convolved with a 2-dimensional gaussian point-spread function. This is an example of the inevitable trade-off between resolution and noise in image reconstruction problems.

The fourier filter may also be employed to compensate for the finite spectral resolution of the data. One simply divides the fourier filter by the fourier transform of the spectral resolution profile. If the spectral resolution profile is a gaussian, its fourier transform is also a gaussian. Since this entails further amplification of high-frequency noise, sharpening of the spectral resolution may not be feasible unless the signal-to-noise ratio of the data are truly superb.

The FFBP algorithm discussed above is essentially the same as the general linear inversion formula given in appendix A of Marsh and Horne (1988). If the trailed-spectrogram data $D(v,\phi)$ is given by a projection of the doppler map $I(V_X, V_Y)$:

$$D(v,\phi) = \int_{-\infty}^{\infty} \int_{-\infty}^{\infty} I(V_X, V_Y) g(v - V_Z + V_X \cos(2\pi\phi) - V_Y \sin(2\pi\phi)) dV_X dV_Y,$$

where $g(v)$ is a (narrow) profile defined by instrumental resolution and local line broadening, then by substituting for $g(v)$ in terms of its Fourier transform $\tilde{g}(\omega)$ we have:

$$D(v,\phi) = \int_{-\infty}^{\infty} \int_{-\infty}^{\infty} I(V_X, V_Y) \int_{-\infty}^{\infty} \tilde{g}(\omega) e^{+i2\pi\omega(v - V_Z + V_X \cos(2\pi\phi) - V_Y \sin(2\pi\phi))} d\omega dV_X dV_Y,$$

and further algebra yields the inversion formula:

$$I(V_X, V_Y) = \int_0^1 \int_{-\infty}^{\infty} \int_0^{\infty} \frac{2\pi\omega}{\tilde{g}(\omega)} D(v,\phi) e^{-i2\pi\omega(v - V_Z + V_X \cos(2\pi\phi) - V_Y \sin(2\pi\phi))} d\omega dv d\phi.$$

We hope that our more lengthy and intuitive treatment, by splitting this inversion formula into two steps, fourier filtering and back-projection, will make the FFBP algorithm easy to understand and use.

Maximum Entropy Methods

The maximum entropy method (MEM) is probably the best way to reconstruct doppler maps from trailed-spectrogram data. The MEM procedure locates the "smoothest" or "simplest" doppler map that fits the data at a specified level of χ^2. A thorough discussion is given by Marsh and Horne (1988), including tests with simulated datasets to illustrate various artefacts due to noise, finite spectral and phase resolution, and so forth. There is flexibility here to include correct treatments of the finite spectral and phase resolution of the data, blending of adjacent spectral lines, occultation effects, and so forth.

MEM requires a sophisticated algorithm to search through the space of all positive maps to find the map with maximum entropy subject to the data consistency constraint. Such algorithms are generally iterative, and require hundreds or thousands of times more computer time than the FFBP algorithm. Since MEM is a non-linear algorithm, it is not simple to follow the propogation of statistical uncertainties from the data to the map, although this may be accomplished (given sufficient computer time) through Monte-Carlo simulations with perturbed datasets. Since MEM requires a positive image, special treatment is required for maps that contain both positive and negative values (emission and absorption lines).

Interpreting Doppler Maps of Cataclysmic Variable Stars

Cataclysmic variable stars produce strong optical emission lines, with double-peaked velocity profiles arising from the nearly-Keplerian orbital motion within the accretion disk. In addition, there are S-wave components from emission-line regions on the companion star and in the accretion stream. What will these regions look like on a doppler map ?

The nearly Keplerian velocity field of the disk gives rise to a distorted “inside-out” image of the disk in the doppler map. Each closed streamline in the disk maps into a closed loop in the doppler map, the doppler radius and azimuth at different positions around the loop being given by the velocity vectors at corresponding positions around the streamline. Gas flowing with constant velocity around a circular orbit will map into a circle with a radius equal to the flow speed. The DISK'S doppler image is inside-out because the outer rim of the disk, where the Kepler velocity is smallest, maps into the inner edge of the doppler image.

The intensity in the disk's doppler image is defined by the line surface brightness at the corresponding position on the face of the disk, multiplied by the Jacobian of the transformation from position to doppler coordinates, and convolved with the spectral resolution and local line broadening profiles. For a Keplerian flow, the Jacobian factor scales as V^{-6}, thus the intensity in the disk's doppler image will be strongly amplified near its inner edge, even if the line surface brightness is much higher in the inner disk. The much larger velocity shear in the inner disk spreads out the emission from this relatively small area into a large annulus on the doppler map.

Since gas in the accretion disk orbits around the white dwarf primary, orbital motion of the white dwarf about the center of mass of the binary system will cause the centroid of the disk's doppler image to be displaced downward on the map to $V_Y = -K_1$, where K_1 is the semi-amplitude of the white dwarf's orbit. This effect may be used to measure K_1, but note that the appearance of the disk's image, and hence its centroid, can be significantly distorted due to deviations of the disk streamlines from pure Keplerian orbits, and to azimuthal variations in the line emissivity.

The mass-losing secondary star in a cataclysmic variable fills its Roche lobe and rotates synchronously with the binary orbit. Because it rotates uniformly, there is no distortion in mapping the secondary star from position to doppler coordinates. Line-forming regions on the secondary star map into a Roche-lobe-shaped region centered at $V_Y = +K_2$, where K_2 is the radial velocity semi-amplitude of the orbit of the secondary star's center of mass. The location of the doppler image of the Roche lobe generally lies inside the inner edge of the doppler image of the disk, since the orbital velocity of the secondary star is less than the Keplerian velocity in the disk.

The core of the gas stream follows a ballistic trajectory starting from the inner Lagrangian point on the secondary star and reaching down to the collision point on the rim of the disk, and perhaps to even smaller radii if the upper fringe of the stream clears the outer rim of the disk and skims over its surface. The expected location of emission from the gas stream may be calculated by integrating the ballistic equations of motion in the rotating frame of the binary starting from the inner Lagrangian point. The velocity vectors at different points along the ballistic trajectory define a curve in the doppler map starting at the image of the inner Lagrangian point, accelerating first in the $-V_X$ direction, and curving toward the $-V_Y$ direction due to the coriolis force. Emission may also be expected at the disk's Keplerian velocity evaluated at locations along the stream trajectory, since the disk material may be excited to emission as the stream material skims across its surface. This second trajectory is similar to the first but is displaced slightly upward.

Doppler Maps of Cataclysmic Variable Stars

The current literature on cataclysmic variable stars holds a small but growing number of doppler tomograms. Hessman (1990) presents a back-projection map of Hβ in the strong-lined cataclysmic variable GD 552. Kaitchuck *et al.* (1990) presents back-projection maps of Hβ in the dwarf nova U Gem at two epochs in quiescence. These back-projections are not true reconstructions, as discussed above, but they do show a broad annulus of emission from the disk, and an enhanced region on the inner edge of the annulus corresponding to the S-wave from the stream–disk interaction region.

Interesting kinematics and ionization structure of the stream–disk interaction region are partially revealed by Marsh *et al.* (1990), who present MEM tomograms for Hβ, Hγ, He I $\lambda4471$ and He II $\lambda4686$ emission in the dwarf nova U Gem at quiescence. The gas stream emission is extended in the Balmer line maps, and there appears to be a slight displacement of the positions of the unresolved He I and He II peaks. The emitting gas has kinematics halfway between the ballistic stream trajectory, and the Keplerian flow at positions along the stream. This indicates that the two flows mix before emitting. Observations with higher velocity resolution are feasible and could resolve the structure of this complex region in detail.

Marsh and Horne (1990) compare MEM tomograms of the dwarf nova IP Peg in outburst and quiescence. These maps show the emergence during outburst of a Balmer line region on the inward-facing side of the companion star, and of He II emission in the accretion disk and wind. Higher velocity resolution can produce doppler maps capable of resolving active regions in the chromosphere of the secondary star.

Perhaps the most important results from doppler mapping studies of cataclysmic variables will be the determination of line ratios and emissivities as a function of radius in the accretion disk, which offer diagnostics of physical conditions in the disk. Results so far show that quiescent accretion disks tend to have Balmer-line surface brightnesses following an $R^{-3/2}$ power-law. Note that this is proportional to the local Kepler rotation frequency. Horne and Saar (1990) point out that a similar linear correlation between emission-line surface brightness and rotation holds for the H α and Ca II H+K emission from the active chromospheres of rotating stars. This leads to a working hypothesis that dynamo action scaling linearly with rotation is the power source for accretion disk chromospheres, as is thought to be the case for rotating stars. Further work is needed to explore this analogy between stellar and disk activity more quantitatively by making maps of disks in different emission lines such as Ca II H,K and Mg II, which are already well studied in stars.

Future Work

Further progress depends on the involvement of many workers to apply doppler mapping techniques to more lines and different types of systems. Higher velocity resolution than has generally been employed in studying the emission lines is feasible and will considerably sharpen up the maps. The narrow emission-line features from the secondary stars in cataclysmic variables would be particularly interesting to map with higher resolution. Are the emission lines seen most strongly on the inward-facing hemisphere are due to irradiation, or to a concentration of active regions near the inner Lagrangian point by surface flows or lower surface gravity there ? Theoretical work predicting line strengths and ratios as functions of radius in accretion disks, and the detailed structure of the stream–disk interaction region will soon be needed to interpret the doppler maps.

It may be worthwhile in closing to discuss two possible extensions of current doppler tomography techniques that appear to be feasible and may soon be implemented, perhaps by readers of this article: error bars and phase-variations.

Unlike the MEM algorithm, the FFBP is a linear algorithm in the sense that each map value is a linear function of the data values. Thus it should be relatively straightforward to propogate the statistical variances of the individual data points through the FFBP process to calculate the statistical variance for each pixel of the FFBP map. The map values are not statistically independent, of course, since we know that varying one of the data points will induce variations in a streak across the map. It may therefore be best to use a full Monte-Carlo simulation to propogate the error bars from the data to any quantity measured from the map. Nevertheless, having an error-bar map may be a helpful shortcut when it comes to extracting quantitative measurements of map features.

Current doppler tomography methods assume that the emission seen from each parcel of gas is independent of the viewing angle around the binary orbit. This assumption would be true for the isotropic emission from optically-thin emission lines, and for absorption lines from an optically-thick disk. But the assumption is certainly violated by occultation effects, and by the shear-induced anisotropy of optically-thick emission lines from the Keplerian accretion disk (Horne and Marsh 1986). The S-wave components from the stream–disk interaction region, and from the companion star, are frequently observed to be strongly modulated with binary phase. Doppler maps currently fit only the mean flux of these components, and the phase variations lead to artefacts. But it may be possible to extend current methods in order to fit the phase-dependent variations. Recall that the back-projection entails computing the mean flux of data sampled along various S-wave velocity curves. The idea is to generalize this to fitting a low-order fourier series to the spectral data sampled along the S-wave. This would yield, for example, a mean value, and amplitudes for the $\sin(2\pi\phi)$ and $\cos(2\pi\phi)$ components of each pixel of the map. A vector field plot of the sine and cosine amplitudes would indicate which S-wave components are significant anisotropic radiators, and in which direction the anisotropic part of their emission is directed. Further work is needed in this area including analysis to see if this approach can be made rigorous, and tests with simulated and real data to ascertain what sort of artefacts may arise.

This work has been supported by NASA grants NAGW-2264 and NAGW-2678.

References

"The Massive, nearly face-on cataclysmic variable GD 552"
Hessman, F. V. and Hopp, U. (1990). *Astron. Astrophys.*, **228**, 387.

"Atlas of Time-resolved Spectrophotometry of Cataclysmic Variables"
Honeycutt, R. K., Kaitchuck, R. H. and Schlegel, E. M. (1987). *Astrophys. J. Suppl.*, **65**, 451.

"Emission Line Formation in Accretion Disks"
Horne, K. and Marsh, T. R. (1986). *Mon.Not.Roy.astron.Soc.*, **218**, 761.

"Rotation and Emission-Lines in Stars and Accretion Disks "
Horne, K. and Saar, S. H. (1991). *Astrophys. J. (Letters)*, **374**, L55.

"Observed Properties of S-Waves"
Kaitchuck, R. H., Schlegel, E. M. and Hantzios, P. A. (1990). *Accretion-Powered Compact Binaries, 11th North American Workshop on Cataclysmic Variables and Low-Mass X-Ray Binaries. Santa Fe 9-13 Oct 1989.* ed. C. Mauche (Cambridge University Press).

"Images of Accretion Discs II. Doppler Tomography"
Marsh, T. R. and Horne, K. (1988). *Mon.Not.Roy.astron.Soc.*, **235**, 269.

"Emission Line Mapping of Dwarf Nova IP Pegasi in Outburst and Quiescence"
Marsh, T. R. and Horne, K. (1990). *Astrophys. J.*, **349**, 593.

"Doppler Imaging of the Dwarf Nova U Geminorum"
Marsh, T. R., Horne, K., Schlegel, E. M., Honeycutt, K. and Kaitchuck, R. H. (1990). *Astrophys. J.*, **364**, 637.

"Doppler Images of Rotating Stars using Maximum Entropy Image Reconstruction"
Vogt, S. S., Penrod, G. D., and Hatzes, A. P. (1987). *Astrophys. J.*, **321**,, 496.